VALIDATION OF A MATHEMATICAL MODEL OF STOCKBRIDGE DAMPER

Renato Barbieri, e-mail: renato.barbieri@pucpr.br
Pontifícia Universidade Católica do Paraná – PUCPR - Curitiba – Brasil

Nilson Barbieri, e-mail: nilson.barbieri@pucpr.br
Pontifícia Universidade Católica do Paraná – PUCPR - Curitiba – Brasil
Universidade Tecnológica Federal do Paraná – UTFPR – Curitiba - Brasil

Oswaldo Honorato de Souza Júnior, e-mail: oswaldo@lactec.org.br
Universidade Tecnológica Federal do Paraná – UTFPR – Curitiba – Brasil
LACTEC- Instituto de Tecnologia para o Desenvolvimento

Vinícius Pereira Silva, e-mail: vinicius@lactec.org.br
LACTEC- Instituto de Tecnologia para o Desenvolvimento

Abstract. *In this work the authors try to establish a procedure to adjust the bending stiffness and the loss factor of the numeric stockbridge damper model using as reference data the experimental FRF (Frequency Response Function) curve. To validate the mathematical model the Genetic Algorithm (GA) method was used to approximate the experimental and numeric FRF curves. To obtain the experimental data were used seven accelerometers displaced along the sample. The experimental and simulated results present good approximations.*
Keywords*: Stockbridge damper, cable, dynamical analysis, parameter estimation*

1. INTRODUCTION

Wind-excited vibrations generated by vortex shedding are very common in high-voltage overhead transmission lines. Although such vibrations are rarely perceptible due to their low amplitudes (less than a conductor diameter), they are, however, extremely important since they may lead to conductor fatigue (Hagedorn et al., 2002). These vibrations are usually caused by winds ranging in velocity from 1 to 10 m/s and can occur at frequencies from 3 to 150 Hz. In conventional transmission line systems, one or more dampers may be attached to a conductor in an effort to suppress aeolian vibrations (Hagedorn et al., 2002).

The Stockbridge damper is presently the most common type of transmission-line damper. In general, a Stockbridge-type damper consists of two weights attached to the end of stranded cables, which are known as *messenger wires*. In this work the behavior of an asymmetric Stockbridge damper with four resonant response frequencies in the range $10 \leq f \leq 60$ Hz is analyzed.

Vecchiarelli, Currie and Havard (2000) introduced an iterative finite-difference scheme to predict the vertical, steady-state, monofrequent, aeolian vibration of a single conductor span with a Stockbridge-type damper attached. This numerical scheme is based on empirical models developed to represent the vortex-induced lift force from the wind as well as the forces of dissipation associated with the conductor self-damping and the damper. The scheme has the capability to account for more than one spatial mode of conductor vibration, travelling-wave effects, conductor flexural rigidity, and damper mass. A two-part numerical analysis is performed in which the "finite-difference scheme is applied to simulate aeolian vibrations of a typical conductor with and without a Stockbridge-type damper.

A detailed mathematical description of conductor motion is difficult due to the stranded construction of a conductor (Vecchiarelli et al., 2000). An example of this problem is the study realized by Nawrocki and Labrosse (2000) where the cable is modeled using each individual wire model and all possible contacts are investigated. Although to get good results for static analysis this model was not applied for dynamic problems and the dynamic friction between the individual wires of the cable was also not studied.

In Stockbridge dampers, mechanical energy is dissipated in wire cables (“damper or messenger cables”). The damping mechanism is due to statical hysteresis resulting from Coulomb (dry) friction between the individual wires of the cable undergoing bending deformation. Systems with statical hysteresis can be modeled by means of Jenkin elements arranged in parallel, consisting of linear springs and Coulomb friction elements. The damper cable is a continuous system and damping takes place throughout the whole length of the cable, so that distributed Jenkin elements are used. Using such a model for the damper cables, the equations of motion can be formulated for a Stockbridge damper, and discretization of the damper cable leads to a system of nonlinear ordinary differential equations. In order to test this dynamical model of a Stockbridge the experimental impedance curves are compared with numeric results (Sauter and Hagedorn, 2002).

Verma (2002) uses masing model for modeling the nonlinear damping behavior of the damper cable of Stockbridge damper. Quasi-static behavior of cable was approximated by considering it as a linearly elastic Euler-Bernoulli beam. Model of damper cable was, then, transferred to the half of the Stockbridge damper body, considering it as symmetric,

for getting the dynamic behavior of damper by determining its impedance. The impedance for different vibrational frequencies were computed. Results for model were then, verified by comparing them with the impedance obtained from experiments on real Stockbridge damper. It was found that the behavior of a damper cable could be reasonably described by using the masing model.

Markiewicz [6] analyzed the optimum dynamic characteristics of Stockbridge dampers for dead-end spans. The analysis showed that the optimum damper impedance required for such spans (called dead-end spans) differs significantly from the optimum impedance of the standard damper and also showed how the efficiency of a standard damper used in such spans may be improved by its proper location on a cable.

Wang et al. (1995) analyzed the free vibration of a transmission line conductor equipped with a number of Stockbridge dampers modeled by a differential equation of motion of a tensioned beam acted on by concentrated frequency dependent forces and an exact solution is obtained using integral transformation.

Espíndola and Silva Neto (2001) using a three-degree of freedom model to modeling the Stockbridge damper, showed the viscoelastic behavior of the flexural stiffness. This model is similar to model used by Sauter and Hagedorn (2002) and Verma (2002).

In contrast of the Sauter and Hagedorn (2002) approach the main idea of this work is to obtain a simple and computational efficient model for the dynamical behavior of Stockbridge damper. The messenger wire is modeled with a simple finite element and the physical parameters (hysteretic damper and the flexural stiffness) are estimated using comparisons with the experimental FRF.

The present study is organized as follows: (i) develop a simple and comprehensive finite element for the messenger wire and the damper weight; (ii) perform a numerical harmonic analysis of the Stockbridge damper; (iii) obtain experimental data using harmonic base excitation; (iv) obtain the error between experimental and numerical results; (v) the complex stiffness parameter is estimated minimizing the error with Genetic Algorithms (Wang et al., 1997) and (vi) the same procedure is repeated for modal approach.

2. MATHEMATICAL MODELS AND RESULTS

In this section are shown the mathematical models of the Stockbridge damper system for two different approaches and the respective results.

2.1. Messenger Wire Model

The messenger wire is modeled using the Euler-Bernoulli beam finite element. In this element the transversal displacement is interpolated using the well-known *Hermitian interpolation polynomials* with C^1 continuity and the degrees of freedom (d.o.f) in each node are the transversal displacement and the rotation, $\{v,\theta\}$. The dynamic equation for this element can be written in the following form:

$$\frac{\rho AL}{420}\begin{bmatrix} 156 & 22L & 54 & -13L \\ & 4L^2 & 13L & -3L^2 \\ & & 156 & -22L \\ \text{sim.} & & & 4L^2 \end{bmatrix}\begin{Bmatrix} \ddot{v}_1 \\ \ddot{\theta}_1 \\ \ddot{v}_2 \\ \ddot{\theta}_2 \end{Bmatrix} + \frac{EI}{L^3}\begin{bmatrix} 12 & 6L & -12 & 6L \\ & 4L^2 & -6L & 2L^2 \\ & & 12 & -6L \\ \text{sim.} & & & 4L^2 \end{bmatrix}\begin{Bmatrix} v_1 \\ \theta_1 \\ v_2 \\ \theta_2 \end{Bmatrix} = -\frac{\rho AL}{12}\begin{Bmatrix} 6 \\ L \\ 6 \\ -L \end{Bmatrix}\ddot{y}_0 \tag{1}$$

where ρA is the linear density of cable, L is the finite element length, EI is a cable flexural (bending) stiffness and $\ddot{y}_0$ is the base acceleration excitation (shaker).

To take in consideration the cable *hysteretic damping* in equation (1) it is sufficient to consider the flexural stiffness as

$$EI = EI_o(1+\beta_i) \tag{2}$$

where β is the *hysteretic damping constant* and $i = \sqrt{-1}$.

The same theory of Euler-Bernoulli and the hysteretic damping had been also used by several authors (Espindola and Silva Neto, 2001; Sauter and Hagedorn, 2002; Verma, 2002; López and Venegas, 2001; Almeida et al, 1992) to modeling this problem. The majority of these authors use only one element of beam to obtain the stiffness matrix.

2.2. Damper Mass Model

The suspended masses of the shock absorber (Stockbridge) are modeled with rigid body plane motion hypothesis and the admissible displacements are shown in the Fig. 1.

After the assembly of all the elements of the messenger wire, each one of the Stockbridge damper weights contributes with two terms for the dynamical equilibrium. The first contribution is in the mass matrix (inertia force)

$$[M_S][\{\ddot{q}_n\}] = \begin{bmatrix} m & m\bar{x} \\ m\bar{x} & I_n \end{bmatrix} \begin{Bmatrix} \ddot{v}_n \\ \ddot{\theta}_n \end{Bmatrix} \tag{3}$$

and another parcel is in the vector force due to base acceleration

$$\{f_s\} = -\begin{Bmatrix} m \\ m\bar{x} \end{Bmatrix} \ddot{y}_0 \tag{4}$$

where m is the mass of Stockbridge damper weight, $\bar{x}$ is the center of mass coordinate and I_n is the inertia moment with reference fixed in node n.

These two terms are obtained using the first variation of the kinetic energy (Hamilton Principles) and the rigid body plane motion hypothesis for suspended Stockbridge damper weight modeling. With the convention defined in the Fig.1, the kinetic energy of each one of the Stockbridge damper weights can be written taking as reference the node n (the node of the finite element mesh connected to the messenger wire). This expression is:

$$T = \frac{1}{2} m \dot{\mathbf{r}}_n \cdot \dot{\mathbf{r}}_n + \dot{\mathbf{r}}_n \cdot [\boldsymbol{\omega} \times m\bar{\mathbf{x}}] + \frac{1}{2} \boldsymbol{\omega} \cdot \int_m \boldsymbol{\rho}_n \times [\boldsymbol{\omega} \times \boldsymbol{\rho}_n] dm \tag{5}$$

where $\dot{\mathbf{r}}_n$ is the velocity of node n, $\boldsymbol{\omega}$ is the damper weight angular velocity and $\boldsymbol{\rho}_n$ is the particle position of dm mass with origin fixed in node n.

Taking in consideration the hypotheses of rigid body plane motion, $\boldsymbol{\omega} = \dot{\theta}_n \mathbf{k}$, and symmetry in y, ($\bar{y}$=0), the expression for kinetic energy of damper weight can be rewrite after integration as:

$$T = \frac{1}{2} m[\dot{u}_n^2 + \dot{v}_n^2 + 2\dot{y}_0 \dot{v}_n + \dot{y}_0^2] + \bar{x} m[\dot{\theta}_n \dot{v}_n + \dot{\theta}_n \dot{y}_0] + \frac{1}{2} I_n \dot{\theta}_n^2 \tag{6}$$

The variation of T can be write as $\delta T = \frac{\partial T}{\partial \dot{u}_n} \delta \dot{u}_n + \frac{\partial T}{\partial \dot{v}_n} \delta \dot{v}_n + \frac{\partial T}{\partial \dot{\theta}_n} \delta \dot{\theta}_n$. Integrating by parts the terms in $\delta \dot{v}_n$ and $\delta \dot{\theta}_n$ and neglecting the boundary terms results the equations (3) and (4).

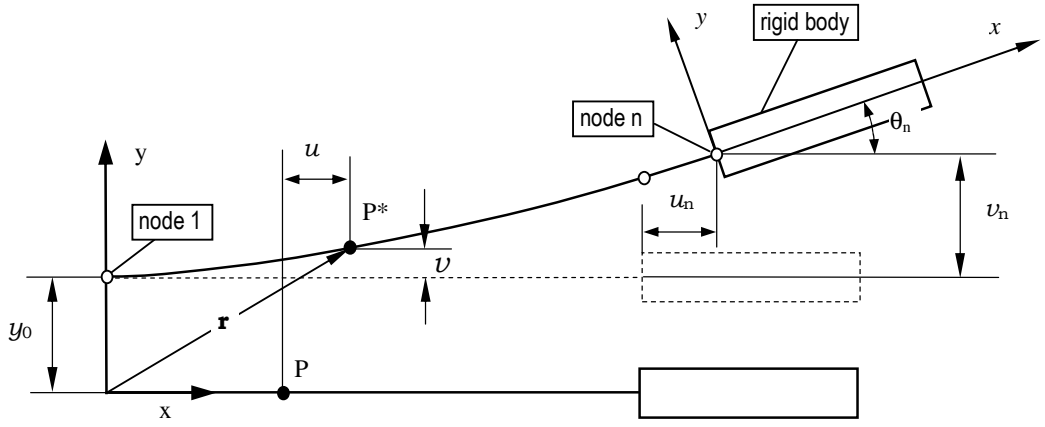

Figure 1 – References and admissible displacements.

2.3. Finite Element System of Equations

The Stockbridge discretized dynamical equilibrium equations is obtained after assembling all finite elements and can be written in the conventional way as

$$[\mathbf{M}]\{\ddot{\mathbf{q}}\}+[\mathbf{K}]\{\mathbf{q}\}=\{\mathbf{f}_0\}\ddot{y}_0(t) \tag{7}$$

where [**M**] and [**K**] are the mass and stiffness matrices and { $\mathbf{f}_0$} is the force vector. The components of vector {**q**} are the finite element node displacements and rotations, *v* and θ; and $\ddot{y}_0$ is the acceleration in node 1 (base shaker acceleration).

Admitting the base excitation as harmonic, $\ddot{y}_0(t)=|\ddot{y}_0|e^{i\omega t}$, the solution **q**(t) is of the form $\mathbf{q}(t)=\mathbf{q}_0 e^{i\omega t}$. Substitution this assumed form of solution into the equation of motion (7) yields:

$$\left[-\omega^2[\mathbf{M}]+[\mathbf{K}]\right]\{\mathbf{q}_0\}=|\ddot{y}_0|\{\mathbf{f}_0\} \tag{8}$$

The amplitude of the displacement vector is calculated solving the Equation (8) for each frequency ω and the amplitude of the acceleration vector is easily calculated with the product ω^2 {$\mathbf{q}_O$}**.** In this work the value $|\ddot{y}_0|=1\ \mathrm{m/s^2}$ was used in all the calculations. Thus, the numerical value of the normalized acceleration $\frac{\omega^2}{|\ddot{y}_0|}\{\mathbf{q}_O\}$ is obtained directly from the finite element vector displacement solutions.

2.4. Experimental set-up

In order to measure the complex flexure stiffness, the asymmetric Stockbridge specimen is mounted to a support placed on an electrodynamics shaker. The scheme of the measurement system for the complex flexure stiffness is shown in Fig.2. However, before the Stockbridge is mounted your clamp is cut on the position indicated in Figure 3a with white line. The objective of this procedure is to eliminate possible measurement errors and to assure greater rigidity for the Stockbridge assembly, Fig. 3b. The characteristics of Stockbridge tested are shown in Table 1.

Table 1 – Stockbridge characteristics.

Properties	Damper mass	
	small	large
$\overline{x}$ [mm]	13,8	27,5
mass [kg]	0,735	0,833
I_{CG} [kg*m^2]	1,8433E-3	1,1631E-3
	Messenger cable	
mass/lenght [kg/m]	0,55	

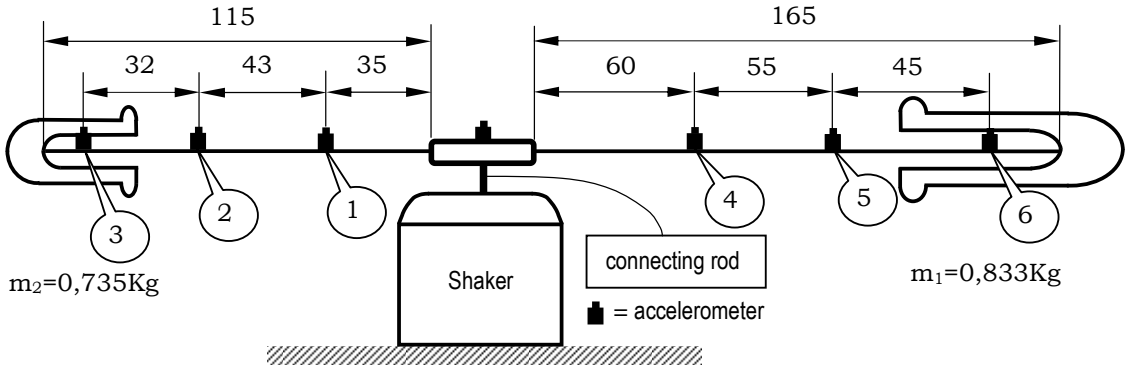

Figure 2 – Schematic diagram of the measurement system for complex flexure stiffness, [mm].

The sensors used in the experimental tests are two capacitance accelerometers KMT ACC B2; two piezoelectric charge accelerometer Bruel & Kjaer 4393 and two ICP PCB 353B33 accelerometers. One PC Spectrum/Network Analyzer Hewlett Packard 3566/67 is used for the experimental signals inputs and the base excitation was made by mean of electromechanical Shaker Gearing & Watson model V350.

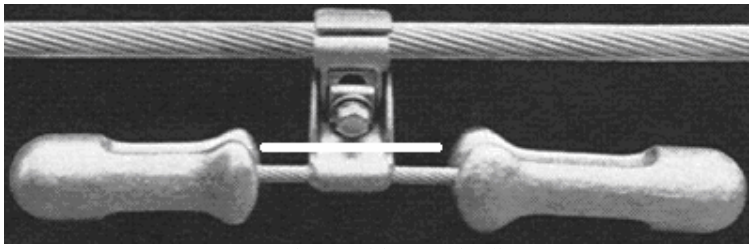

(a) Cutting position (white line)

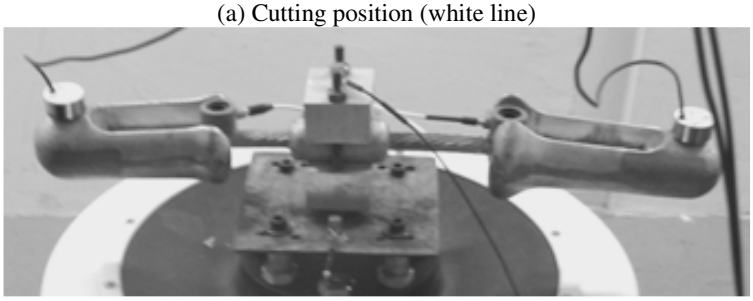

(b) Assembly detail

Figure 3 – Stockbridge assembly.

2.5. GAs Optimization

The complex dynamic flexural stiffness value has been estimated for the messenger wire using the procedure reported in the following. The procedure is based on the GAs minimization of the objective function

$$f(EI_0,\beta) = \left| \text{real}\left|\frac{\ddot{q}_n}{\ddot{y}_0}\right|_{EXP} - \text{real}\left|\frac{\ddot{q}_n}{\ddot{y}_0}\right|_{FEM} \right| + \left| \text{imag}\left|\frac{\ddot{q}_n}{\ddot{y}_0}\right|_{EXP} - \text{imag}\left|\frac{\ddot{q}_n}{\ddot{y}_0}\right|_{FEM} \right| \tag{9}$$

where the subscript n indicate the finite element node with coordinate equal to the accelerometer position and the subscripts EXP and FEM indicate the experimental and numerical values of the normalized acceleration, respectively.

The principal GAs parameters used in this work is show in Table 2. The pair (EI_0,β) is considered one solution when the tolerance indicated in Table 2 is reached or when the limit of generations is exceeded. The excellent solution is when the objective function value is less than the convergence tolerance.

Table 2 – GAs Parameters

Parameter	value
Number of Bits	24
Number of Family	20
Maximum number of generations	2000
Crossover Probability	1
Mutation probability	0,02
Convergence tolerance, ε	10^{-3}

2.6. Frequency domain results

In the Fig. 4 we show the values for the complex flexural stiffness (real and imaginary part) and for the objective function obtained using de optimization process described previously. The necessary experimental data for the objective function definition are collected in accelerometer placed in position 2 indicated in Figure 2 and the numerical values are obtained using homogeneous finite element mesh with 40 elements.

It is observed that the variation of the EI(ω) imaginary part is greater than the variation of the EI(ω) real part. This behavior is due to the fact of that the excitation in frequencies near to the resonance produce great displacements and this can affect the hysteretic damping of the system.

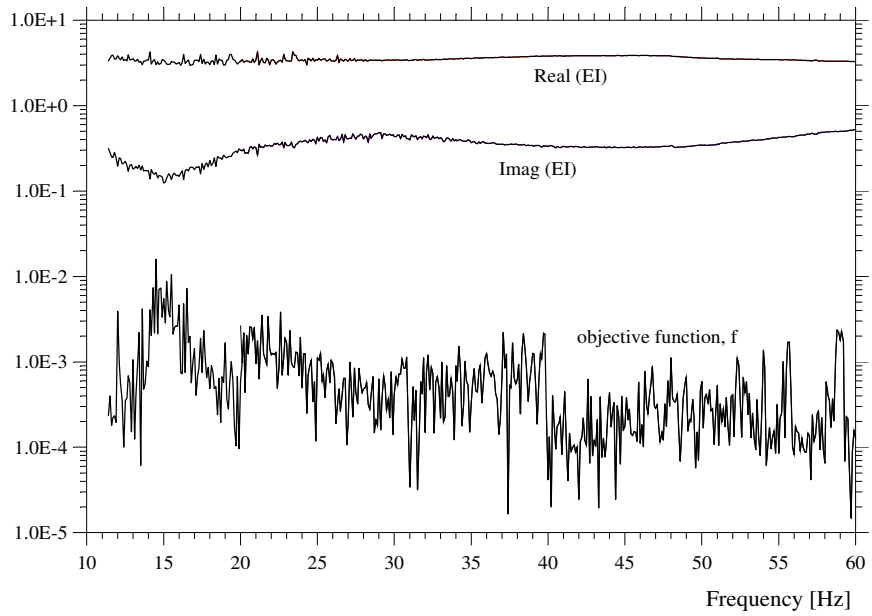

Figure 4 – Optimum values estimated with experimental data collected in the position 2.

Figure 5 shows the normalized acceleration for position 3 (small mass). The experimental results were obtained through the accelerometer 3 and the numeric results were obtained using the parameters estimated for the position 2. The error between these two curves is greater than the values of the objective function shown in Fig. 6. However, the two curves also are close and these results indicate that the adjustment for position 2 is sufficiently satisfactory.

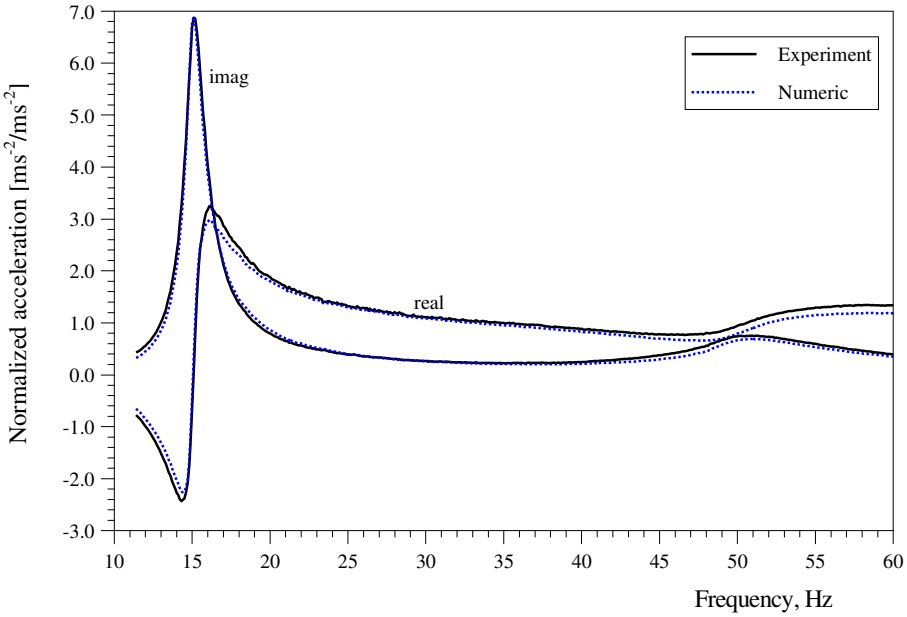

Figure 5 – Normalized acceleration comparison for the small mass in the position 3.

Figure 7 shows the results for the flexural stiffness obtained with normalized acceleration error optimization for accelerometers 1 and 2. These results present good agreement with some small differences in low frequencies.

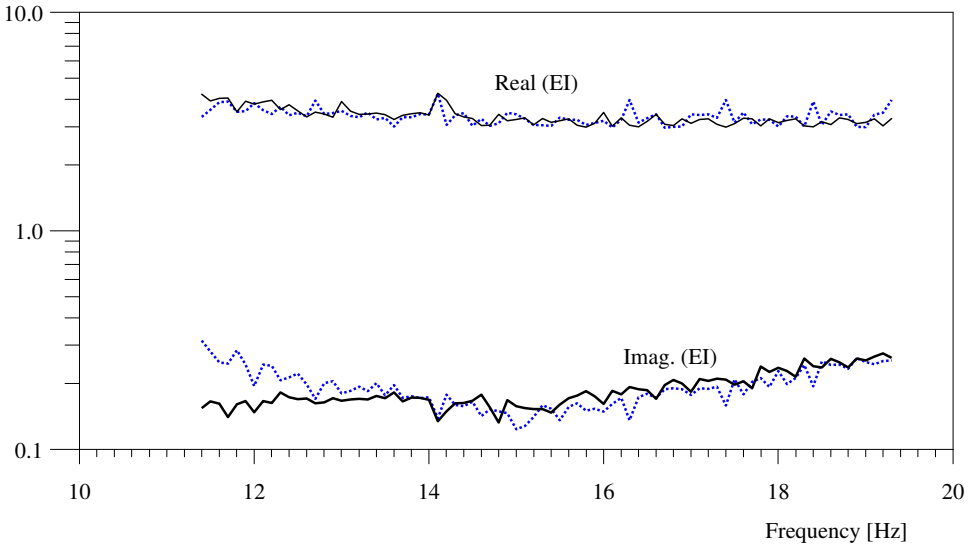

Figure 6 – Optimum values estimated with experimental data collected in the positions 1 (continuous line) and 2 (dashed line).

Figure 7 shows the values of complex flexural stiffness obtained with experimental data for the position 6. These results shows lower value fluctuations and good agreement with the results obtained for other positions illustrated in Figs. 4 to 6.

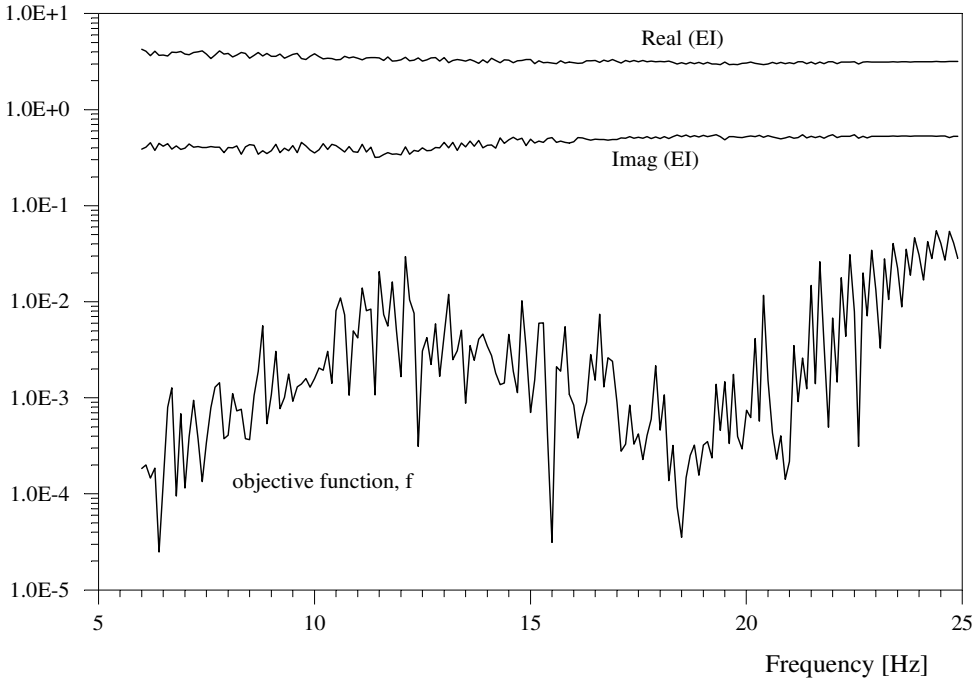

Figure 7 – Optimum values estimated with experimental data collected in the position 6.

2.7. Modal Approach

Let $\mathbf{v}_1$ and $\mathbf{v}_2$ two different eigenvector associated with ω_1 and ω_2 of the undamped system:

$$\left[-\omega^2[\mathbf{M}]+real[\mathbf{K}]\right]\{\mathbf{v}_j\}=\{\mathbf{0}\} \tag{10}$$

such that

$$\begin{bmatrix}\mathbf{v}_1 & \mathbf{v}_2\end{bmatrix}^t[\mathbf{K}]\begin{bmatrix}\mathbf{v}_1 & \mathbf{v}_2\end{bmatrix}\begin{Bmatrix}y_1\\ y_2\end{Bmatrix}=\begin{bmatrix}k_1 & 0\\ 0 & k_2\end{bmatrix}\begin{Bmatrix}y_1\\ y_2\end{Bmatrix} \tag{11}$$

and

$$\begin{bmatrix}\mathbf{v}_1 & \mathbf{v}_2\end{bmatrix}^t[\mathbf{M}]\begin{bmatrix}\mathbf{v}_1 & \mathbf{v}_2\end{bmatrix}\begin{Bmatrix}\ddot{y}_1\\ \ddot{y}_2\end{Bmatrix}=\begin{bmatrix}1 & 0\\ 0 & 1\end{bmatrix}\begin{Bmatrix}\ddot{y}_1\\ \ddot{y}_2\end{Bmatrix} \tag{12}$$

The matrix *real*[**K**] depends on the value of EI_0, then the first stage of the modal analysis is to evaluate this value. In this work the GAs was used in these calculations. The experimental and numerical values of the two first natural frequencies of the system are used to define the objective function and its mathematical expression is:

$$f(EI_0)=\left(\omega_{1\,EXP}-\omega_{1\,MEF}\right)^2+\left(\omega_{2\,EXP}-\omega_{2\,MEF}\right)^2 \tag{13}$$

where $\omega_{i\,exp}$ and $\omega_{i\,MEF}$ are the ω_i experimental and numeric values of ω_i, respectively. The experimental FRF attains its maximum value at the resonant frequency (*hysteretic damping*) while the numeric values are obtained using the Subspace Iteration Method.

Considering the coordinate transformation

$$\mathbf{q}=\begin{bmatrix}\mathbf{v}_1 & \mathbf{v}_2\end{bmatrix}\begin{Bmatrix}y_1\\ y_2\end{Bmatrix} \tag{14}$$

and replacing now Equation (14) into (7) and pre-multiplying by $\begin{bmatrix}\mathbf{v}_1 & \mathbf{v}_2\end{bmatrix}^t$ can be obtained:

$$\begin{bmatrix}k_1 & 0\\ 0 & k_2\end{bmatrix}\begin{Bmatrix}y_1\\ y_2\end{Bmatrix}+\beta(\omega)\begin{bmatrix}k_1 & 0\\ 0 & k_2\end{bmatrix}\begin{Bmatrix}\dot{y}_1\\ \dot{y}_2\end{Bmatrix}+\begin{bmatrix}1 & 0\\ 0 & 1\end{bmatrix}\begin{Bmatrix}\ddot{y}_1\\ \ddot{y}_2\end{Bmatrix}=\begin{Bmatrix}f_1\\ f_2\end{Bmatrix}\ddot{y}_0 \tag{15}$$

where $\begin{Bmatrix}f_1 & f_2\end{Bmatrix}^t=\begin{bmatrix}\mathbf{v}_1 & \mathbf{v}_2\end{bmatrix}^t\{\mathbf{f}\}$.

Taking by hypothesis the approximation,

$$\beta(\omega)\begin{bmatrix}k_1 & 0\\ 0 & k_2\end{bmatrix}=\begin{bmatrix}\beta_1 k_1 & 0\\ 0 & \beta_2 k_2\end{bmatrix} \tag{16}$$

The equation (15) can be rewrite as

$$\begin{bmatrix}k_1 & 0\\ 0 & k_2\end{bmatrix}\begin{Bmatrix}y_1\\ y_2\end{Bmatrix}+\begin{bmatrix}\beta_1 k_1 & 0\\ 0 & \beta_2 k_2\end{bmatrix}\begin{Bmatrix}\dot{y}_1\\ \dot{y}_2\end{Bmatrix}+\begin{bmatrix}1 & 0\\ 0 & 1\end{bmatrix}\begin{Bmatrix}\ddot{y}_1\\ \ddot{y}_2\end{Bmatrix}=\begin{Bmatrix}f_1\\ f_2\end{Bmatrix}\ddot{y}_0 \tag{17}$$

which is a set of independent equations and the parameter β_j may be understood as an *modal hysteretic damping constant*.

If the base excitation is harmonic the equation relative to mode j is

$$k_j y_j+\frac{\beta_j k_j}{\omega}\dot{y}_j+\ddot{y}_j=-f_j\left|\ddot{y}_0\right|e^{i\omega t}\qquad j=1,2. \tag{18}$$

Equation (18) is solved by assuming a solution of the form $y_j(t)=Y_j e^{i\omega t}$, where Y_j is constant. Substitution of this in equation (18) yields

$$(k_j+i\beta_j k_j-\omega^2)Y_j e^{i\omega t}=-f_j\left|\ddot{y}_0\right|e^{i\omega t}\qquad j=1,2. \tag{19}$$

and solving this expression for the amplitude Y_j results:

$$\left|Y_j\right| = \frac{\left|\ddot{y}_0\right|}{k_j} \frac{f_j}{\sqrt{(1-r_j^2)^2 + \beta_j^2)}} \tag{20}$$

where $r_j = \omega/\omega_j$.

The physical node displacement, $q_n(t)$, and the acceleration, $\ddot{q}_n(t)$, are calculated using the coordinate transformation, Equation (14), and can be obtained:

$$q_n(t) = a_1 y_1(t) + a_2 y_2(t) = (a_1 Y_1 + a_2 Y_2) e^{i\omega t} = Q_n e^{i\omega t} \tag{21}$$

and

$$\ddot{q}_n(t) = a_1 \ddot{y}_1(t) + a_2 \ddot{y}_2(t) = -\omega^2 (a_1 Y_1 + a_2 Y_2) e^{i\omega t} = -\omega^2 Q_n e^{i\omega t} \tag{22}$$

where a_1 and a_2 are the v_1 and v_2 node displacement value, respectively.

The experimental and the numerical values of the normalized acceleration, $\left|\ddot{q}_n\right| / \left|\ddot{y}_0\right|$, are used to obtain β_1 and β_2 parameters. The best values for β_1 and β_2 are obtained by GAs minimization of the objective function defined as

$$f(\beta_1, \beta_2) = \sum_{j=1}^{np} abs\left(\left| \frac{\ddot{q}_n}{\ddot{y}_0} \right|_{EXP} - \left| \frac{\ddot{q}_n}{\ddot{y}_0} \right|_{FEM} \right) \tag{23}$$

where np is the number of experimental points.

2.8. Modal Analysis result

Figure 8 shows the experimental normalized acceleration for the position 2 and the numeric values obtained with the modal analysis described previously. The frequency range $10 \leq f \leq 55$ Hz is used in the objective function minimization and the parameters EI_o, β_1 and β_2 were maintained constant. This fact justifies the high value of β_1 visualized clearly in Fig. 8 near the first natural frequency. The optimal estimated parameters values are $EI_o = 4.4172$ Nm^2, β_1=0.1554 and β_2 = 0.3259. These values are close to the values found by Espíndola e Silva Neto (2001).

Although the numerical and experimental curves presents few differences the modal constant parameters estimation approach is worse than the frequency dependent parameters EI_0 and β estimation. In this work it was not carried out the modal analysis with frequency dependent parameters EI_o, β_1 and β_2.

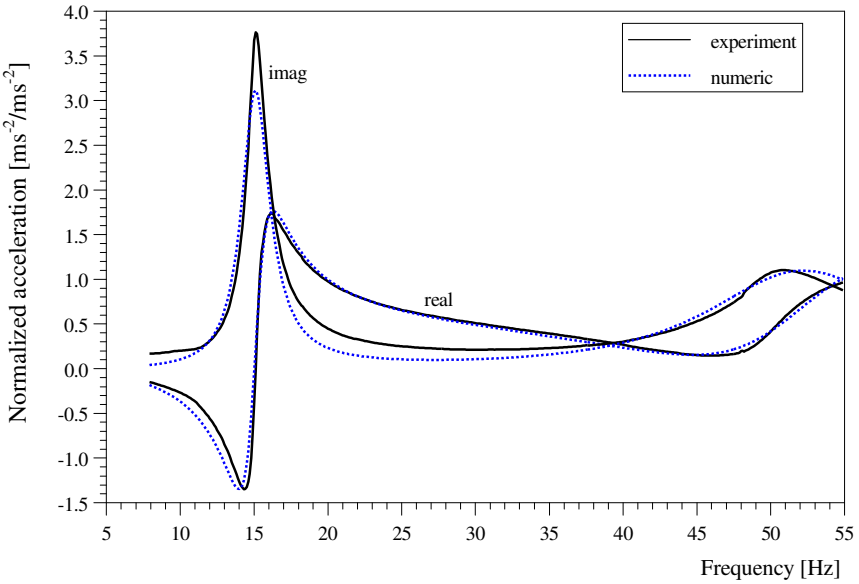

Figure 8 – Normalized acceleration comparison for the position 2.

3. CONCLUSIONS

In this work were used two different approaches to investigate the dynamical behavior of Stockbridge damper: frequency dependent parameters and modal analysis. The main conclusions obtained with the results are:

- The proposed simple model was able to estimate with efficiency the dynamical response of studied Stockbridge.
- The frequency domain analysis with EI_0 and β variables produces good results.
- The adjustment with modal analysis with constant parameters EI_o, β_1 and β_2 also produced satisfactory results.
- The small number of design variables and the simple mathematical model with lower band width obtained through finite elements for the messenger wire are essential for the GAs implementation with good computational efficiency and accuracy.
- Although the shown results are very good, more studies are necessary to get robust models for the messenger wire with individual wire localized contact and for the damper mass nonlinear dynamics.

According López and Venegas (2001), *the experimental test showed that the dimensionless coefficient of damping decreases linearly respect to the amplitude of excitation* and the values found by these authors for the hysteretic damping varies between to 0.1 and 0.678.

4. REFERENCES

Almeida, M. T., Fuchs, R. D., Labegalini, P. R., Labegalini, J. A., 1992, "Projetos Mecânicos das Linhas de Transmissão", Edgard Blücher, São Paulo-SP.

Chang, W.-D., 2006, "An improved real-coded genetic algorithm for parameters estimation of nonlinear systems", Mech. Syst. Signal Proc., Vol. 20, pp. 236–246.

Espíndola, J. J. and Silva Neto, J. M., 2001, "Identification of Flexural Stiffness Parameters of Beams", J. Braz. Soc. Mech. Sci., Vol. 23, pp. 217-225.

Hagedorn, P., Mitra, N. and Hadulla, T., 2002, "Vortex–excited vibrations in bundled conductors: a mathematical model", Journal of Fluids and Structures, Vol. 16, pp. 843–854.

López, A. L., Venegas, J. C., 2001, " Endurance of dampers for electric conductors", International Journal of Fatigue, Vol. 23, pp. 21-28.

Markiewicz, M., 1995, "Optimum dynamic characteristics of Stockbridge dampers for dead-end spans", Journal of Sound and Vibration, Vol. 188, pp. 243-256.

Nawrocki, A., and Labrosse, M., 2000, "A finite element model for simple straight wire rope strands", Computers and Structures, Vol. 77, pp. 345-359.

Sauter, D. and Hagedorn, P., 2002, "On the hysteresis of wire cables in Stockbridge dampers", International Journal of Non-Linear Mechanics, Vol. 37, pp. 1453-1459.

Vecchiarelli, J., Currie I. G. and Havards, D. G., 2000, "Computational analysis of aeolian conductor vibration with a Stockbridge-type damper", Journal of Fluids and Structures, Vol. 14, pp. 489-509.

Verma, H., 2002, "The Stockbridge damper as a continuous hysteric system in single overhead transmission lines", Master Dissertation, Indian Institute of Technology Bombay, 81p.

Wang, H. Q., Miao, J. C., Luo, J. H., Huang, F. and Wang, L. G., 1997, "The free vibration of long-span transmission line conductors with dampers", Journal of Sound and Vibration, Vol. 208, pp. 501-516.

5. RESPONSIBILITY NOTICE

The authors are the only responsible for the printed material included in this paper.